Role of stacking faults in the structural and magnetic properties of ball-milled cobalt

J. Sort,[1] S. Suriñach,[1] J. S. Muñoz,[1] M. D. Baró,[1,*] M. Wojcik,[2] E. Jedryka,[2] S. Nadolski,[2] N. Sheludko,[3] and J. Nogués[4]
[1]*Departament de Física, Universitat Autònoma de Barcelona, 08193 Bellaterra, Spain*
[2]*Institute of Physics, Polish Academy of Sciences, 02 668 Warszawa, Poland*
[3]*Faculty of Physics, University of Sofia, 1126 Sofia, Bulgaria*
[4]*Institució Catalana de Recerca i Estudis Avançats (ICREA) and Departament de Física, Universitat Autònoma de Barcelona, 08193 Bellaterra, Spain*
(Received 22 January 2003; published 16 July 2003)

Stacking faults are found to play a crucial role in the evolution of the structural and magnetic properties of cobalt subjected to ball milling. This has been evidenced by using complementary techniques, i.e., magnetometry and torque measurements, nuclear magnetic resonance (NMR) and x-ray diffraction (XRD). After short milling times a stacking-fault driven transformation from fcc to hcp cobalt is observed, which is accompanied by an increase of the effective magnetic anisotropy, the NMR restoring field and the coercivity. The results suggest that small amounts of stacking faults can be beneficial to enhance the coercivity in hexagonal Co. For longer milling times, both XRD and NMR results show that the hcp phase becomes heavily distorted because of the large amount of stacking faults accumulated. This induces a decrease of the magnetic anisotropy, which leads to the overall softening of the material.

DOI: 10.1103/PhysRevB.68.014421 PACS number(s): 75.50.Tt, 82.56.−b, 61.72.Nn, 67.80.Jd

INTRODUCTION

The cobalt allotropic phase transformations between hexagonal close packed (hcp) and face centered cubic (fcc) have been extensively studied both from the theoretical[1] and experimental points of view.[2] In particular, these transformations can be induced in Co by ball milling.[3,4] Recently, it has been demonstrated that the milling induced hcp-fcc transformation is governed by a process of stacking fault accumulation.[4] However, the magnetic changes in Co accompanying the structural transitions induced during the milling have not been systematically studied. Stacking faults are known to play a crucial role in the magnetic properties of Co-based hexagonal alloys (e.g., longitudinal and perpendicular recording media) and are usually considered to bring about a magnetic softening of this kind of materials.[5,6] However, small amounts of defects seem to improve some of the magnetic properties of other hexagonal Co alloys, e.g., ball milled $SmCo_5$.[7] Thus, a better understanding of the correlation between the structural and magnetic properties of Co based alloys is important for the advancement of their applications.

It is well known that mechanical milling is a widespread technique for the production of nonequilibrium states.[8] In particular, ball milling has been shown to be an excellent process to introduce large amounts of defects in metals in a controlled way, by adjusting the milling conditions, e.g., the milling energy (milling frequency, ball-to-powder ratio), milling atmosphere or milling time.[9]

It is also noteworthy that although nuclear magnetic resonance (NMR) is particularly suited to study the structural and magnetic properties of Co and Co-based alloys,[10] it has not been used to investigate the structural and magnetic transformations induced in Co by ball milling. Since NMR renders information about the local environment of the atoms it often complements the results obtained from macroscopic structural or magnetic techniques such as x-ray diffraction or magnetization.

In the present work we correlate the milling induced structural transformations with the evolution of the magnetic properties in Co from a microscopic (i.e., NMR) and macroscopic points of views. The results indicate that the milling induced stacking faults determine the structural and magnetic properties of Co, hence the appropriate control of the stacking faults can lead to the improvement of the magnetic properties.

EXPERIMENTAL PROCEDURE

Cobalt powders (99.5%, −325 mesh, from Alfa-Aesar ®) were mechanically milled in a planetary ball mill (Fritsch Pulverissette 7), at 500 rpm, during times ranging from 0.1 to 20 h, using agate vials ($V=20$ ml) and six agate balls (with diameter $\phi=10$ mm) in a ball-to-powder weight ratio of 2:1. To avoid oxidation, the vials were previously sealed under argon atmosphere. The as-milled powders were structurally characterized by x-ray diffraction (XRD), using Cu-K_α radiation, and nuclear magnetic resonance. From the XRD patterns, microstructural parameters, such as crystallite sizes, microstrains or stacking faults were quantified by means of a data analysis program based on a full pattern fitting procedure (Rietveld method).[11,12] In particular, crystallite sizes, $\langle D\rangle$, and microstrains, $\langle \varepsilon^2\rangle^{1/2}$, were determined using the Delft model,[11] while stacking fault probabilities were evaluated according to the Warren formulas.[13] ^{59}Co NMR spectra were recorded in a zero external dc field, at room temperature, every 1 MHz, in the frequency range 205–230 MHz, by means of an automated, frequency swept spin-echo spectrometer. Prior to NMR experiments, the as-milled powders were embedded in a polymeric resin and aligned during the resin hardening under a magnetic field ($H=8$ kOe). All magnetic measurements were performed in oriented powders. For each sample, several NMR spectra were taken us-

ing different values of the excitation rf field, h_1, applied parallel to the particle alignment direction. The details of the NMR experimental procedure have been described in Ref. 14. This procedure provides a twofold information about the studied samples. On the one hand, it gives a NMR spectrum that has been corrected for the intrinsic NMR enhancement factor and thus reflects a true number of nuclei resonating at a given frequency. The ^{59}Co NMR frequency can be readily interpreted as fingerprints of different structural components (fcc, hcp, and stacking faults), consequently the structural information can be extracted in a straightforward way.[10,14] On the other hand, the applied experimental procedure provides a distribution of local restoring fields acting on the electronic magnetization in different structural components present in a sample. In this way a microscopic *magnetic* information is obtained in addition to the *structural* information.

Coercivity values were determined by means of vibrating sample magnetometry (VSM), using a maximum field of $H = 11$ kOe. The hysteresis loops were measured at room temperature along the easy axis of the oriented samples.

Finally, to evaluate the effective magnetic anisotropy, torque curves were recorded at room temperature in a compensated torque balance, applying magnetic fields up to $H = 11$ kOe, on disk-shaped oriented samples. The magnetic anisotropy constant, K_U, was determined from the torque curve slope method. This method of determining K_U is especially useful when complete saturation of the disks cannot be guaranteed.[15]

RESULTS AND DISCUSSION

Structural

Shown in Fig. 1(a) are the XRD patterns of cobalt powders before milling and after milling for 0.1, 0.5, 2, and 20 h. Figure 1(b) shows the XRD pattern of a cobalt ball milled for 20 h, together with the curve generated from the full pattern fitting procedure and the corresponding difference between the calculated and the experimental profiles. Also indicated in the figure are the Miller indexes (*hkl*) of the different diffraction peaks, where the subscripts *C* and *H* denote the fcc and hcp phases, respectively.

As can be seen in Fig. 1(a), the unmilled powders are a mixture of hcp and fcc cobalt. However, the amount of fcc rapidly reduces with milling time, as evidenced by the decrease in intensity of the fcc peaks, for example of the $(200)_C$ peak [indicated by an arrow in Fig. 1(a)]. Note that this peak disappears almost completely after milling for 0.5 h. Actually, the amount of fcc decreases from about 35% (wt %) in the unmilled state to about 5% after milling for 0.5 h. Remarkably, after long-term milling, a small hump is observed at the position of this peak. Moreover, XRD patterns reveal that the hcp peaks satisfying the condition $h-k=3n+1$ (where n is an integer) and $l \neq 0$ [for example the $(102)_H$ or $(103)_H$ peaks] are extra broadened with respect to the other peaks [see Fig. 1(b)]. This is an indication of the existence of stacking faults.[13] At the same time, Fig. 1(a) shows that as milling time increases, all the XRD peaks progressively broaden. This results from the crystallite size refinement and the increase of the microstrains. Actually, from the widths of the hcp peaks it is possible to obtain the milling time dependence of both the hcp crystallite size, $\langle D \rangle_H$, and the microstrains in the hcp crystals, $\langle \varepsilon^2 \rangle_H^{1/2}$. However, for the fcc phase, reliable values of $\langle D \rangle_C$ and $\langle \varepsilon^2 \rangle_C^{1/2}$ can be only determined for short milling times, due to the exceedingly small amount of fcc phase present for longer milling times. Thus, in unmilled Co, the crystallite sizes are of about $\langle D \rangle_H = 67.6$ nm and $\langle D \rangle_C = 80.4$ nm for the hcp and fcc phases, respectively, while after milling for 20 h their size

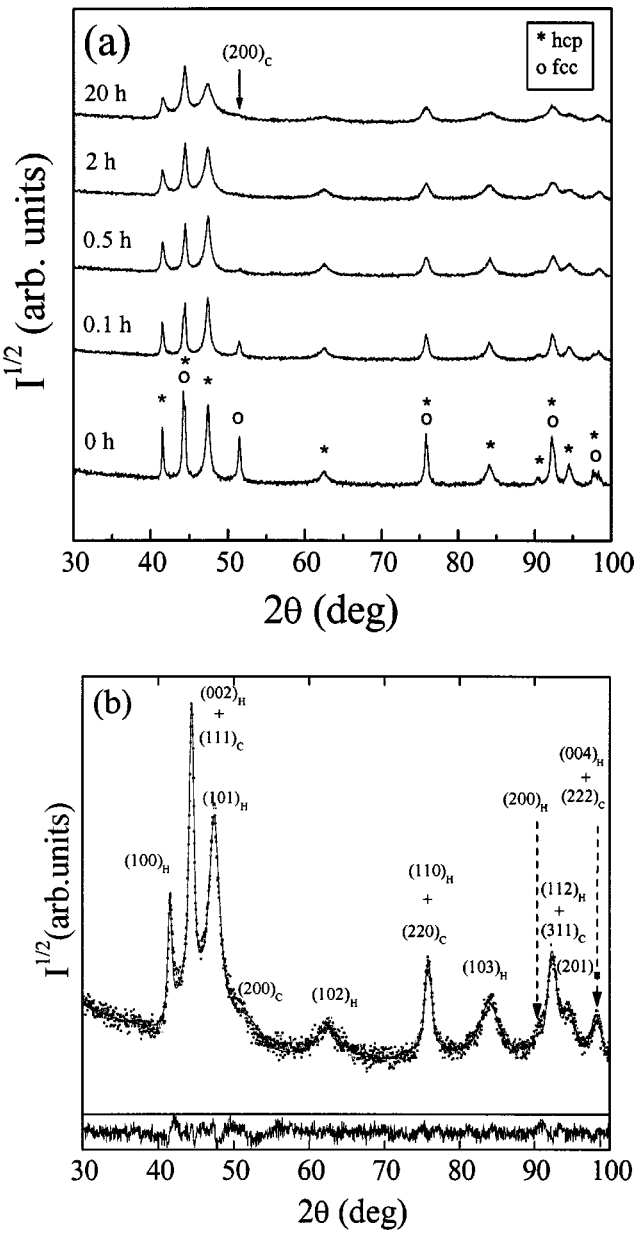

FIG. 1. (a) X-ray diffraction patterns of Co particles before and after milling for 0.1, 0.5, 2, and 20 h. The symbols* and ○ denote the peaks corresponding to hcp and fcc-Co, respectively. (b) X-ray diffraction pattern of 20-h ball milled Co, together with the curve generated from the Rietveld refinement and the corresponding difference between the experimental and calculated profiles. The Miller indexes of the different peaks are also indicated, where *H* and *C* subindexes denote hcp and fcc phases, respectively.

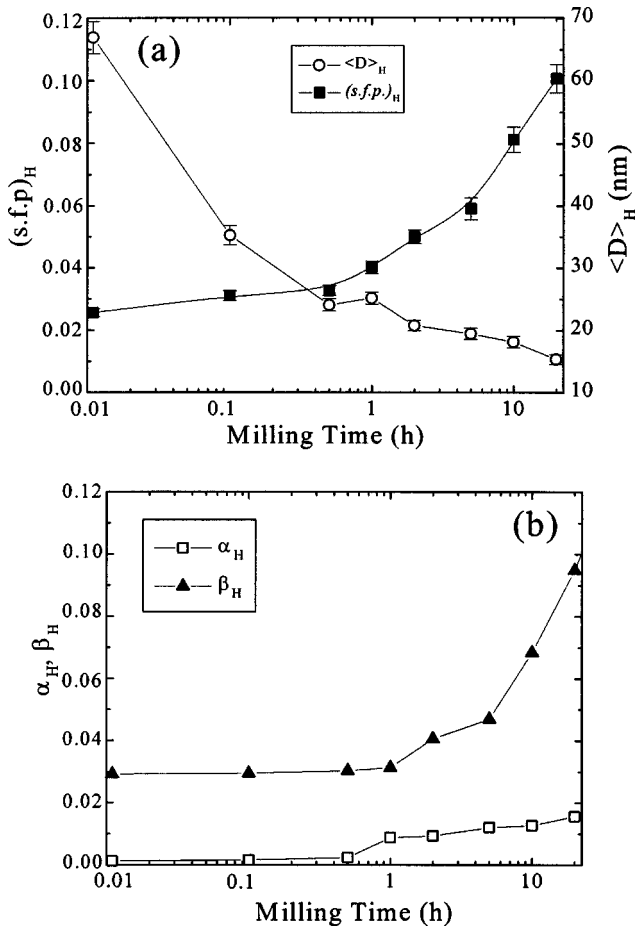

FIG. 2. Milling time dependence of (a) the overall stacking fault probability $(\text{s.f.p.})_H$, and the crystallite size, $\langle D\rangle_H$, of the majority hcp phase and (b) the deformation-type, α_H, and twin-type, β_H, stacking fault probabilities for hcp-Co. Note that $(\text{s.f.p.})_H=\alpha_H+\beta_H$. The lines are guides to the eye.

become $\langle D\rangle_H=16.1$ nm and $\langle D\rangle_C\sim 3$ nm. The milling time dependence of $\langle D\rangle_H$ and the overall stacking fault probability in the hcp phase, $(\text{s.f.p.})_H$, in as-milled cobalt are shown in Fig. 2(a). According to Warren's formulas, $1/(\text{s.f.p.})_H$ indicates the average number of compact atomic planes (in the hcp sequence ...*ABABAB*...) between two consecutive stacking faults.[13] For example, s.f.p.$=0.05$ (i.e. 1/s.f.p.$=20$) indicates that between two stacking faults there are, in average, 20 ordered planes. Actually two different types of stacking faults, deformation, α, and twin, β, faults, are created both in the hcp and fcc phases during the milling, which are related to the slip and twin mechanisms of plastic deformation, respectively.[16,17] These two types of faults bring about different alterations of the hcp and fcc stacking sequences. Thus, in the hcp phase, twin faults result in the ...*ABABCBCB*... sequence, i.e., locally a single fcc stacking order (*ABC*) is generated. This new sequence can be denoted as (…*hhchh*…), where *h* and *c* indicate hcp and fcc local stacking sequence, respectively. On the contrary, deformation faults in hcp phase result in two consecutive alterations of the hcp stacking order. In this case the sequence generated is (…*ABABCACA*…), i.e., (…*hhcchh*…). These two types of faults can be quantified using the Rietveld method, since they have different effects on the XRD patterns.[13]

Shown in the Fig. 2(b) are the milling time dependences of deformation, α_H, and twin, β_H, faults in the hcp structure. It is important to stress that in the hcp phase of the unmilled Co some stacking faults, s.f.p.~ 0.03, are already present, while they are found to be negligible in the fcc phase. Note that the stacking fault probability, $(\text{s.f.p.})_H$, in Fig. 2(a) corresponds to the sum of both types of stacking faults in hcp-Co, $(\text{s.f.p.})_H=\alpha_H+\beta_H$. The stacking faults in fcc-Co also increase after short-term milling (e.g., $\alpha_C+\beta_C\sim 0.04$ after milling for 0.5 h). Nevertheless, since for these milling times the percentage of the remaining fcc-Co is very small (e.g., 5% after milling for 0.5 h) their contribution to the overall amount of stacking faults is negligible. As can be seen in Fig. 2(b), twin-type stacking faults are found to predominate, especially after long-term milling, indicating that twinning, rather than simple slip, is the main mechanism governing plastic deformation of the Co crystallites during the milling.[4] This is probably because in hcp metals, due to the limited number of slip systems, the yield stress for twinning becomes lower than the yield stress for slip under conditions of rapid rate of loading, such as ball milling.[16]

In addition, $\langle\varepsilon^2\rangle_H^{1/2}$ increases with milling time. In the starting material, $\langle\varepsilon^2\rangle^{1/2}$ is found to be approximately zero in both hcp and fcc phases. However, for hcp, $\langle\varepsilon^2\rangle_H^{1/2}$ increases steeply during the first 2 h of milling, followed by a smoother increase for longer milling times, reaching a maximum value of about 0.0064 after long-term milling. Similar values of $\langle\varepsilon^2\rangle_C^{1/2}$ are found for fcc-Co after long-term milling.[4] The high values of $\langle\varepsilon^2\rangle_H^{1/2}$ and $\langle\varepsilon^2\rangle_C^{1/2}$ are probably due to the high density of dislocations and grain boundaries developed during the milling process.

Figure 3 shows the NMR spectra for unmilled Co, and Co milled for 0.1, 0.5, 2, and 20 h. As can be seen in the figure, the NMR spectrum for the initial material exhibits peaks corresponding to fcc-Co, hcp-Co, and different types of stacking faults (sf_1, sf_2, sf_3, sf_4, and sf_5).[10,14] The different stacking fault frequencies are usually assigned as follows: (i) sf_1 and sf_2—one stacking error in the fcc sequence, i.e., fcc twin faults or, alternatively, two consecutive stacking errors in the hcp sequence, i.e., deformation faults in hcp; (ii) sf_3 and sf_4, corresponding to one stacking error in hcp, i.e., twin faults in hcp, or two stacking faults in fcc, i.e., deformation faults in fcc; and (iii) sf_5 is not unambiguously assigned to any stacking error sequence, although these sequences are often related to stacking faults in hcp.[18] The spectrum for the unmilled material (Fig. 3) seems to indicate an excess of fcc phase, compared to the results of the XRD analysis. However, taking into account that in the unmilled Co the hcp phase is already intrinsically highly faulted, contrary to the fcc phase, the observed NMR intensity at the frequency corresponding to undistorted hcp Co should be smaller. Moreover, one should bear in mind that since the penetration depth of the r.f. field used in the NMR experiment is limited, and that fcc-Co tends to be retained at the surface of the particles during a thermally-induced fcc→hcp transition,[19] a reduced intensity for the unfaulted hcp-Co should also be

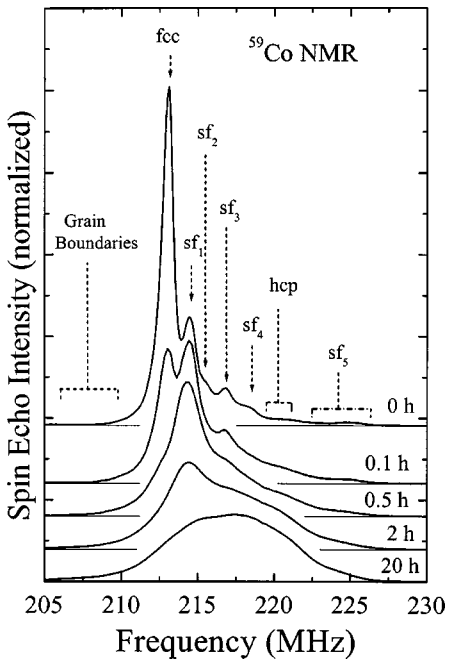

FIG. 3. Room-temperature NMR spectra of unmilled Co and Co milled for 0.1, 0.5, 2, and 20 h. Indicated in the figure are the peaks corresponding to fcc-Co, hcp-Co, and the different types of stacking faults (sf_1, sf_2, sf_3, sf_4, and sf_5). The long tail at low frequencies originates from the grain boundaries contribution. Note that the different spectra have been shifted for clarity.

expected. As the milling time increases, the peak corresponding to fcc-Co quickly disappears, becoming almost indiscernible after 0.5 h of milling, similar to what is observed in XRD. In addition, the relative integral intensity of the peaks corresponding to the different types of stacking faults rapidly increases with milling time. In particular, for short milling times the sf_1 and sf_2 peaks increase, in agreement with the XRD results [Fig. 2(b)], where for short milling times an increase of deformation faults in hcp-Co (i.e., two stacking errors in the hcp sequence) is observed, while maintaining the amounts of twin faults in hcp almost constant. For long milling times, sf_3+sf_4 appear to be predominant, i.e., suggesting that single stacking error in the hcp becomes dominant, as observed for XRD, where twinning, β_H, is the prevailing mechanism for plastic deformation. Also noteworthy is the enhancement of the low frequency tail, corresponding to grain boundaries, with increasing milling time, in accordance with the decreased crystallite size and increase of microstrains observed in XRD. Although a quantitative analysis of the different phases is, in principle, possible, due to the broadening and the concomitant severe overlap of some of the peaks, after 0.5 h of milling such analysis becomes increasingly unreliable. Hence, it has not been attempted.

When comparing XRD and NMR structural results, one can see there is a clear qualitative agreement between both techniques. Namely, there is an obvious transformation of the initial fcc-Co into stacking faults and an increase of disorder, i.e., overall increase of stacking faults or grain boundary regions (e.g., microstrains in XRD), with milling time. However, a more quantitative comparison between NMR and XRD becomes difficult. For instance, although the general trends are the same, there is not necessarily a one-to-one correspondence as to the exact amount of the different structural phases with milling time between the results obtained by NMR and XRD. These discrepancies have several origins. First, a fundamental one is that while NMR is a microscopic technique giving information about the local environment of the atoms, XRD is a more macroscopic technique rendering more long-range information. Stemming from this fundamental distinction it is not surprising that a given stacking sequence could be considered differently in NMR or XRD. One clear example of this is the apparent increase of fcc-Co content observed in XRD after long term milling, e.g., an increase of the $(200)_C$ XRD peak [see Fig. 1(a)]. When looking at the 20-h NMR spectrum, there is no indication of fcc-Co, instead an increase of stacking faults is observed. Thus, taking into account both results and the rather small XRD crystallite size of the fcc-Co, $\langle D\rangle_C(20\,\mathrm{h})\sim 3$ nm, the new state created after long-term milling should be considered as a pseudo-random sequence of stacking faults, still maintaining an overall hcp character, rather than two well differentiated hcp and fcc phases.

Magnetic properties

Since the saturation magnetization of hcp and fcc Co is almost the same,[20] there is virtually no change in the saturation magnetization, M_S, with milling time. However, the bulk anisotropies of hcp and fcc Co are rather different [K_1 (hcp) $=5\cdot 10^6$ erg/cm^3 (Ref. 21) and K_1 (fcc) $=0.8\cdot 10^6$erg/cm^3 (Ref. 22)]. As can be seen in Fig. 4(a) the uniaxial anisotropy, K_U (Ref. 23) and the coercivity, H_C, exhibit an increase for short milling times reaching a maximum for 0.5 h of milling and slowly decreasing for longer milling times. The initial increase of anisotropy with milling time can be understood qualitatively by the stacking-fault driven transformation of fcc Co (low anisotropy) into hcp Co (high anisotropy). Moreover, the microstrains induced during the milling could also influence the anisotropy (e.g., stress induced anisotropy[24]). It is noteworthy that the maximum anisotropy observed in the milled powders is slightly larger than that of bulk hcp Co, which is probably related to the crystallite size refinement induced during the milling, since in Co the surface anisotropy effects could also be significant.[25] However, the decrease in K_U observed for longer milling times is exceedingly large to be related solely to the reverse hcp-fcc transformation. For milling times longer than 1 h large amounts of stacking faults are accumulated in the material. Hence, since stacking faults are known to decrease the anisotropy in Co-based hexagonal materials, it seems plausible to correlate the K_U reduction for long milling times with the increasing amounts of stacking faults and the concomitant disorder. Although the samples have been embedded in resin and oriented, the oriented particles are always composed of several misoriented crystallites. Therefore, the effect of averaging the anisotropy of the different crystallites over the effective exchange length (i.e., random anisotropy model) (Ref. 26) could also be reflected in the reduction of the anisotropy, especially for small crys-

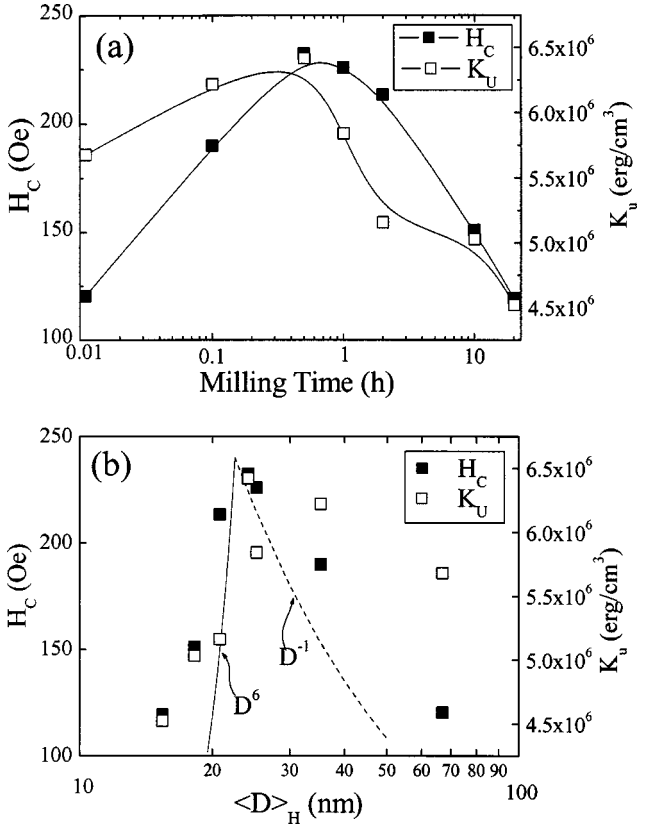

FIG. 4. (a) Milling time dependence of the coercivity, H_C, and uniaxial effective anisotropy, K_U. (b) Dependence of H_C and K_U on the hcp crystallite size, $\langle D\rangle_H$. Note that the lines in (a) are just guides to the eye, while in (b) they indicate $\langle D\rangle^6$ and $\langle D\rangle^{-1}$ dependencies.

tallite sizes (i.e., long milling times). Actually, the random anisotropy model predicts a reduction of the anisotropy, K_U, by a factor $N^{1/2}$, N being the number of grains in a volume $(\ell_{ex})^3$, where ℓ_{ex} denotes the exchange length, which is defined as $(A/K_U)^{1/2}$ (where A is the exchange stiffness). This would lead to an effective anisotropy $\langle K\rangle = K_U/N^{1/2}$. However, in Co the exchange length is about $\ell_{ex}\sim 4.5$ nm (when using bulk K_U values), thus smaller than the observed hcp crystallite sizes, even if the smallest measured effective anisotropy is used to obtain ℓ_{ex}. Hence, the averaging effect should be small. As can be seen in Fig. 4(b), the measured K_U does not follow the expected dependence with $\langle D\rangle_H$ (i.e., $K_U \propto \langle D\rangle_H^6$ for $\langle D\rangle_H < \ell_{ex}$ and $K_U \propto \langle D\rangle^{-1}$ for $\langle D\rangle_H > \ell_{ex}$ (Ref. 26) from the random anisotropy model.

It is well known that coercivity and anisotropy are closely related. For example, if the reversal of the magnetization takes place by coherent rotation, coercivity and anisotropy should be proportional to each other, i.e., $H_C = 2K_U/M_S$.[27] However, as it can be inferred from Fig. 4(a), while the total increase of anisotropy after 0.5 h of milling is merely 13%, the enhancement of the coercivity is almost 100%. Thus, the increase of coercivity cannot be explained only by the increase of anisotropy. One possibility for the anomalous increase of H_C could be a strong exchange coupling between the fcc and hcp phases.[28] Namely, due to the strong exchange

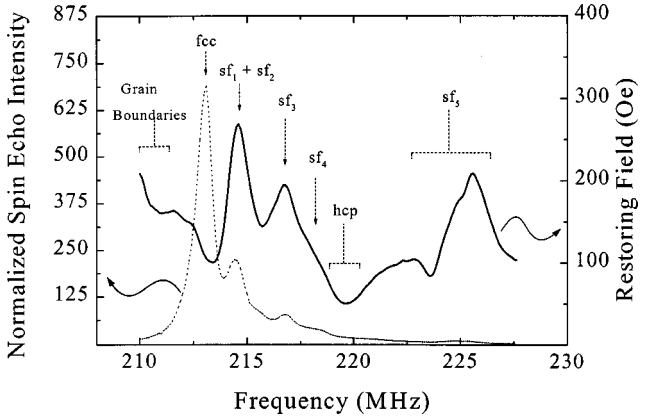

FIG. 5. NMR spectrum of unmilled Co (dotted line) together with the frequency dependence of the normalized restoring field (continuous line). The signal ranges corresponding to the different structural features (undistorted fcc and hcp phases, stacking faults and grain boundaries) have also been indicated.

coupling, when the low coercivity (i.e., low K_U) fcc grains reversed their magnetization, they would also induce the reversal of the high coercivity (i.e., high K_U) hcp grains at lower fields, thus reducing the measured H_C. Therefore, as the amount of fcc phase decreased this effect should be less significant and the hcp grains would reverse at their intrinsic, higher, coercivity. Exploring other possibilities one is led to take into account the pinning of the domain walls by stacking faults and other defects, which would bring about an increase of H_C.[29] This mechanism would be most effective when the average distance between different stacking faults is larger than the domain wall thickness. Consequently, when the amount of stacking faults surpasses a certain limit, the role of the stacking faults or other defects would merely be to reduce the anisotropy, by creating structural inhomogeneities. Hence, the decrease of H_C for long milling times appears to be related to the reduction of K_U, since for long milling times the reduction of both properties is of the same order of magnitude. Finally, the random anisotropy model effects could also influence the behavior of the coercivity with milling time due to the crystallite size reduction. However, similarly to K_U, although these effects should be present they are probably not significant. Consequently, the dependence of H_C on $\langle D\rangle$ is not the one expected from the random anisotropy model[26] [Fig. 4(b)], as observed for K_U.

NMR provides *local* magnetic information complementary to macroscopic magnetization and torque measurements. As can be seen in Fig. 5, for the unmilled material, each structural feature identified by NMR (i.e., fcc, hcp, stacking faults, or grain boundaries) has its specific restoring field. This indicates that the *local* magnetic stiffness, i.e., to a certain extent the difficulty for magnetization reversal, is different at different parts of the Co particles. In particular, the restoring field appears to be largest at different kinds of defects, stacking faults or grain boundaries than at the ordered phases. Moreover, the evolution of the restoring field with milling time, shown in Fig. 6, indicates that for the first milling stages the restoring field curves shift upwards, indicating an overall increase of the magnetic stiffness of the

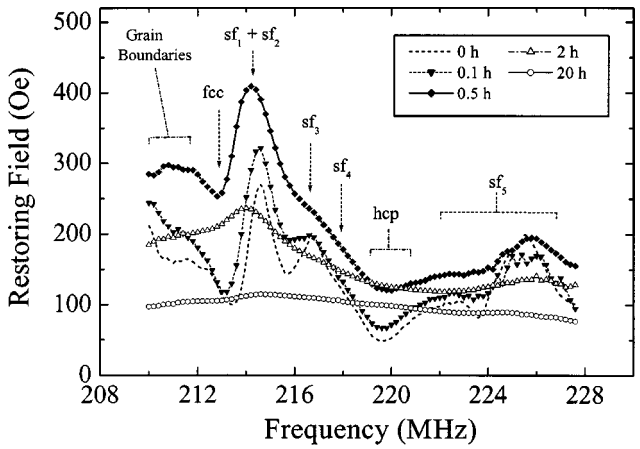

FIG. 6. Frequency dependence of the restoring field of unmilled Co and Co milled for 0.1, 0.5, 2, and 20 h. The frequency ranges corresponding to the different structural features (undistorted fcc and hcp phases, stacking faults and grain boundaries) have also been indicated.

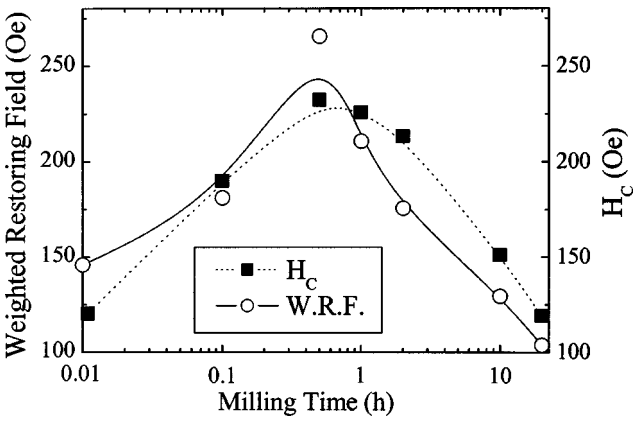

FIG. 7. Milling time dependence of the coercivity, H_C, and the weighted restoring field (W.R.F.), obtained by convoluting the spin echo intensity with the restoring field curve. Note that the lines are guides to the eye.

powders. Interestingly, the stacking faults remain the stiffest structural element of the samples. However, for longer milling times the restoring field curve decreases and broadens out, hence the overall magnetic stiffness decreases, while the difference in magnetic stiffness between the different structural elements smoothens. Finally, for the longest milling time, 20 h, the restoring field becomes virtually featureless.

These results agree well with the anisotropy and coercivity values. As the milling starts, the restoring field increases significantly, in agreement with the coercivity (rather than the anisotropy). Moreover, the fact that the stacking faults are the stiffest part of the restoring field spectrum implies that stacking faults play an important role in the magnetic hardening of the material, probably as domain wall pinning sites. For longer milling times, the smoothing of the restoring field spectrum implies that the stacking faults tend to have less influence in the magnetization reversal, i.e., the increasing amount of stacking faults limits their role as pining sites. It is noteworthy that occasionally, in Co-based hexagonal systems slight increases of coercivity have been observed for small amounts of stacking faults, even though they were not studied in detail.[6] Our study indicates that these coercivity enhancements may be relevant and that small amounts of stacking faults may be beneficial for the improvement of performance in Co-based longitudinal and perpendicular recording media.

To carry out a more quantitative comparison between the microscopic (restoring field) and macroscopic (H_C and K_U) we have integrated the convolution of the spin echo intensity and restoring field curve,[30] which renders a ''weighted'' restoring field, i.e., the average magnetic stiffness of the whole sample, hence somewhat equivalent to the macroscopic coercivity. As can be seen in Fig. 7, the weighted restoring field corresponds closely to the coercivity values (Fig. 4).

Finally, it is important to stress that the results from microscopic (NMR) and macroscopic (XRD and magnetometry) studies have been proven to be rather complementary. This fact helps to better understand the correlation between the structural and magnetic effects in this system.

CONCLUSION

The evolution of the structural and magnetic properties of Co when subject to ball milling have been studied using local (NMR) and macroscopic averaging (XRD, VSM, and torque magnetometry) techniques. The results indicate that both the structural (allotropic phase transformations) and magnetic (evolution of the anisotropy and the coercivity) properties of Co are mainly dominated by the stacking faults induced during the milling. In particular, the results show that small amounts of stacking faults can be used to enhance the coercivity of Co-based hexagonal alloys. Finally, this study evidences the complementariety of the NMR, XRD, and magnetometry techniques to fully understand the role of stacking faults in the properties of ball milled Co.

ACKNOWLEDGMENTS

The authors wish to thank L. Lutterotti for providing the Rietveld XRD refinement program. J.S. thanks the DGU for its financial support. Partial support from CICYT (MAT2001-2555), DGR (2001SGR00189) and a grant from Ford Motor Company to the NMR group in Warsaw are also acknowledged.

*Corresponding author. Email address: dolors.baro@uab.es. Fax: +34-93-5812155

[1] S. Mahajan, M. L. Green, and D. Brasen, Metall. Trans. A **8**, 283 (1977); V. P. Dmitriev, S. B. Rochal, Y. M. Gufan, and P. Tolédano, Phys. Rev. Lett. **62**, 2495 (1989); P. Tolédano, G. Krexner, M. Prem, H. P. Weber, and V. P. Dmitriev, Phys. Rev. B **64**, 144104 (2001).

[2] C. R. Houska, B. L. Averbach, and M. Cohen, Acta Metall. **8**, 81 (1960); H. Schumann, Z. Metallkd. **60**, 322 (1969); S. Kajiwara, S. Ohno, and K. Honma, Philos. Mag. A **63**, 625 (1991); C.

Kuhrt and L. Schultz, J. Appl. Phys. **73**, 6588 (1993).
[3] M. Baricco, N. Cowlam, L. Schiffini, P. P. Macri, R. Frattini, and S. Enzo, Philos. Mag. B **68**, 957 (1993); F. Cardellini and G. Mazzone, Philos. Mag. A **67**, 1289 (1993); J. Y. Huang, Y. K. Wu, and H. Q. Ye, Acta Mater. **44**, 1201 (1996); J. Sort, J. Nogués, X. Amils, S. Suriñach, J. S. Muñoz, and M. D. Baró, Appl. Phys. Lett. **75**, 3177 (1999).
[4] J. Sort, J. Nogués, S. Suriñach, and M. D. Baró, Philos. Mag. A **83**, 439 (2003); J. Sort, N. M. Mateescu, J. Nogués, S. Suriñach, and M. D. Baró, J. Metastable Nanocryst. Mater. **12**, 126 (2002).
[5] B. Bian, W. Yang, D. E. Laughlin, and D. N. Lambeth, IEEE Trans. Magn. **37**, 1456 (2001); L. Holloway and H. Laidler, IEEE Trans. Magn. **37**, 1459 (2001); Y. Takahashi, K. Tanahashi, and Y. Hosoe, J. Appl. Phys. **91**, 8022 (2002).
[6] P. Dova, H. Laidler, K. O'Grady, M. F. Toney, and M. F. Doerner, J. Appl. Phys. **85**, 2775 (1999); B. Y. Wong, Y. Shen, and D. E. Laughlin, *ibid.* **73**, 418 (1993); L. Holloway and H. Laidler, *ibid.* **87**, 5690 (2000); T. M. Coughlin, E. R. Wuori, and J. H. Judy, J. Vac. Sci. Technol. **20**, 171 (1982).
[7] D. L. Leslie-Pelecky and R. L. Schalek, Phys. Rev. B **59**, 457 (1999); J. Sort, S. Suriñach, J. S. Muñoz, M. D. Baró, J. Nogués, G. Chouteau, V. Skumryev, and G. C. Hadjipanayis, *ibid.* **65**, 174420 (2002).
[8] B. S. Murty and S. Ranganathan, Int. Mater. Rev. **43**, 101 (1998).
[9] H. J. Fetch, E. Hellstern, Z. Fu, and W. L. Johnson, Metall. Trans. A **21**, 2333 (1990); D. G. Morris and A. Benghalem, Mater. Sci. Forum **179–181**, 11 (1995); Á. Révész and J. Lendvai, Nanostruct. Mater. **10**, 13 (1998); D. G. Morris, X. Amils, J. Nogués, S. Suriñach, M. D. Baró, and M. A. Muñoz-Morris, Int. J. Non-Equilib. Process. **11**, 379 (2002).
[10] P. Panissod, in *Frontiers in Magnetism of Reduced Dimensions Systems*, edited by V. G. Bar'yakhtar, P. E. Wigen, and N. A. Lesnik (Kluwer, Amsterdam, 1998), p. 225; C. Mény, E. Jedryka, and P. Panissod, J. Phys.: Condens. Matter **5**, 1547 (1993); P. Panissod, J. P. Jay, C. Meny, M. Wojcik, and E. Jedryka, Hyperfine Interact. **97/98**, 75 (1996); M. Cerisier, K. Attenborough, E. Jedryka, M. Wojcik, S. Nadolski, C. Van Haesendonck, and J. P. Celis, J. Appl. Phys. **89**, 7083 (2001).
[11] R. A. Young, *The Rietveld Method* (Oxford University Press, New York, 1995).
[12] L. Lutterotti and P. Scardi, J. Appl. Crystallogr. **23**, 246 (1990); L. Lutterotti and S. Gialanella, Acta Mater. **46**, 101 (1997).
[13] B. E. Warren, *X-Ray Diffraction* (Addison-Wesley, Reading, MA, 1969).
[14] P. Panissod, M. Malinowska, E. Jedryka, M. Wojcik, S. Nadolski, M. Knobel, and J. E. Schmidt, Phys. Rev. B **63**, 012102 (2001).
[15] H. P. Klein, A. Menth, and R. S. Perkins, Physica B & C **80**, 153 (1975).
[16] G. E. Dieter, *Mechanical Metallurgy* (McGraw-Hill, London, 1988).
[17] R. W. Hertzberg, *Deformation and Fracture Mechanics of Engineering Materials* (Wiley, New York, 1996).
[18] L. E. Toth and S. F. Ravitz, J. Phys. Chem. Solids **24**, 1203 (1963); H. Brömer and H. L. Huber, J. Magn. Magn. Mater. **8**, 61 (1978).
[19] M. Erbudak, E. Wetli, M. Hochstrasser, D. Pescia, and D. D. Vvedensky, Phys. Rev. Lett. **79**, 1893 (1997).
[20] M_S (hcp) = 161.9 emu/g and M_S (fcc) = 164.8 emu/g. S. Chikazumi, *Physics of Ferromagnetism* (Oxford University Press, New York, 1997), Appendix 4.
[21] The given value is the bulk hcp K_1 anisotropy. R. Skomski and J. M. D. Coey, *Permanent Magnetism* (Institute of Physics, Bristol, 1999).
[22] Since bulk fcc Co is not stable at room temperature the value given for K_1 (fcc) is a rough estimate from the literature values on fcc-Co thin films, which are rather spread. Nevertheless, it is well accepted that K_1 (fcc) is 5–10 times smaller than K_1 (hcp) at room temperature. R. M. Osgood III, K. T. Riggs, A. E. Johnson, J. E. Mattson, C. H. Sowers, and S. D. Bader, Phys. Rev. B **56**, 2627 (1997); D. Weller, G. R. Harp, R. F. C. Farrow, A. Cebollada, and J. Sticht, Phys. Rev. Lett. **72**, 2097 (1994).
[23] Note that since the samples are not single phase the anisotropy constant obtained from torque is not purely the hcp K_1 of Co, but rather an average uniaxial anisotropy in the direction of the sample alignment.
[24] S. Chikazumi, *Physics of Magnetism* (Wiley, New York, 1964).
[25] M. Jamet, W. Wernsdorfer, C. Thirion, D. Mailly, V. Dupuis, P. Mélinon, and A. Pérez, Phys. Rev. Lett. **86**, 4676 (2001).
[26] G. Herzer, IEEE Trans. Magn. **26**, 1397 (1990); K. Suzuki and J. M. Cadogan, Phys. Rev. B **58**, 2730 (1998); J. Löffler, J. P. Meier, B. Doudin, J. P. Ansermet, and W. Wagner, *ibid.* **57**, 2915 (1998); R. Alben, J. J. Becker, and M. C. Chi, J. Appl. Phys. **49**, 1653 (1978).
[27] E. C. Stoner and E. P. Wohlfarth, Philos. Trans. R. Soc. London, Ser. A **240**, 599 (1948).
[28] E. F. Kneller and R. Hawig, IEEE Trans. Magn. **27**, 3588 (1991).
[29] R. Skomski and J. M. D. Coey, *Permanent Magnetism* (Institute of Physics, Bristol, 1999).
[30] Note that the convolution, $\int I_{SE} H_{Rest} d\omega$, (where I_{SE} is the spin echo intensity and H_{Rest} the restoring field) is necessary in order to properly carry out the weighted average to account for the different amount of the diverse structural elements. For example, even grain boundaries have a rather large restoring field, since for short milling times they are only a tiny fraction of the spin echo spectrum they do not contribute significantly to the average restoring field.